Rare Metal Materials and Engineering
Volume 50, Issue 10, October 2021
Available online at www.rmme.ac.cn

Science Press

Cite this article as: Zuo Min, Li Yongli, Xia Wenli, et al. Novel Synthesis of Multistage Porous Ni-P Particles Through Cu-Ni-P Alloys[J]. Rare Metal Materials and Engineering, 2021, 50(10): 3512-3519.

ARTICLE

Novel Synthesis of Multistage Porous Ni-P Particles Through Cu-Ni-P Alloys

Zuo Min, Li Yongli, Xia Wenli, Zhao Degang, Wang Yan

School of Materials Science and Engineering, University of Jinan, Jinan 250022, China

Abstract: Cu-Ni-P alloys with different atomic ratios of Ni: P (2: 1, 3: 1, 4: 1 and 5: 1) were designed, and the microstructure characteristics and phase extraction treatments of ingots and melt-spun ribbons were discussed. Results show that Cu-*x*Ni-4.5P ingots are composed of Cu and multiple Ni-P phases, including Ni_5P_4, $Ni_{12}P_5$ and Ni_3P. With melt-spun process, the phosphides mainly exist in the form of $Ni_{12}P_5$ and Ni_3P compounds. Meanwhile, further increasing nickel concentration of alloys can cause the structure-coarsening of phosphides in some degree. By controlling the solidification behavior and phase extraction process, Ni-P particles with multistage pore structure can be obtained, in which the pores are formed due to the etching of Cu dendrites and Cu existing in eutectic structure and solid solution region. Thus, phase extraction from metallic alloys provides a new controllable method to synthesize functional multistage porous phosphides.

Key words: transition metal phosphides; Ni-P; microstructure; multistage pore; phase extraction

Recently, the synthesis of hydrogen, as an alternative energy source, has drawn considerable attention. However, the slow kinetics of oxygen evolution reaction (OER) at the anode has become a considerable obstacle to the hydrogen production process, and Pt-group materials were used as the preferred catalyst due to their excellent activity and long-lasting durability[1, 2]. The rising cost of Pt has resulted in significant efforts to find low-cost alternatives.

Transition-metal phosphides (TMPs) have been considered as optimal substitutes for electrode materials for energy conversion and energy storage owing to their typical metalloid features, rather high activity and chemical stability[3, 4]. Among these compounds, nickel phosphides with multiple stoichiometric ratios are the most remarkable products because of their significant role in the catalytic field, including Ni_2P, Ni_3P, Ni_5P_2, Ni_8P_3 and $Ni_{12}P_5$[5 - 8]. Now there are some wonderful researching results focused on the controllable synthesis methods. Mi et al[9] achieved $Ni_{12}P_5$ and Ni_2P selective preparation using a solvothermal route with nickel chloride and white phosphorus as the starting reactants. Tian et al [10] reported an alternative approach to obtain Ni_2P with a sulfur-containing surface through reduction of nickel hexathiodiphosphate ($Ni_2P_2S_6$). Ledendecker et al[11] synthesized a highly ordered Ni_5P_4 with nanoarchitectures on Ni foil through a contact-conversion system. Furthermore, the controllable synthesis of nickel phosphides with various sizes, phase composition and morphologies has gained increasing attention, which may have a remarkable impact on the catalytic performance. Based on these reports, it is found that an effective strategy for improving catalytic efficiency and electrochemical performance is to construct phosphides with high specific surface area, and to possess multistage porous structure is even better[12, 13].

To obtain porous structures, especially nanoporous structures, the electrochemical and chemical dealloying have been recognized as the optimal methods based on the difference in standard electrochemical potentials of components and the tunable porous structure can be obtained through changing the microstructure and composition of precursor and dealloying process parameters[14,15]. This highly effective approach has been widely applied to fabricate various nanoporous systems, mainly including Pt[14], Au[16,17],

Received date: March 24, 2021
Foundation item: Natural Science Foundation of Shandong Province (ZR2019MEM019); National Natural Science Foundations of China (51772132); Shandong Province Higher Educational Youths Innovative Science and Technology Program (2019KJA018)
Corresponding author: Zuo Min, Ph. D., Associate Professor, School of Materials Science and Engineering, University of Jinan, Jinan 250022, P. R. China, Tel: 0086-531-82765473, E-mail: mse_zuom@ujn.edu.cn

Ag[18], Cu[19], Ni[20] and Pd[21]. Recently, some researchers have gradually discovered that functional phosphides can be successfully synthesized using dealloying routes[22, 23].

In contrast to those conventional dealloying systems, novel synthesis of honeycomb Ni-P compounds through phase extraction of Cu-Ni-P alloys was reported. This versatile route not only benefits the simple and convenient recovery of element phosphorus but also acts as a promising synthetic method for hierarchical porous materials. Meanwhile, the influences of atomic ratio between Ni and P and dealloying process parameters on the phase composition and structure characteristic of Cu-Ni-P systems were also discussed.

1 Experiment

1.1 Materials and processing

The highly pure Cu, Ni and Cu-14P alloys were used to prepare a series of Cu-Ni-P alloys in a vacuum arc melting furnace under argon atmosphere (all compositions quoted in this work are in mass fraction unless otherwise stated). The phosphorus was added in the form of Cu-14P master alloy, which was supplied by Hunan Rare Earth Metal Research Institute. Based on different atomic ratios of Ni/P as 2∶1, 3∶1, 4∶1 and 5∶1, a series of Cu-Ni-P alloys were designed, including Cu-17.1Ni-4.5P, Cu-25.6Ni-4.5P, Cu-34.1Ni-4.5P and Cu-42.6Ni-4.5P. In arc melting furnace, the raw materials were melted four to five times to obtain the optimal compositional homogeneity of alloys. Subsequently, Cu-Ni-P alloys molten in quartz tubes were quenched by a rotating Cu roller with a speed of 1000~2500 r/min, and a series of Cu-Ni-P ribbons were obtained.

1.2 Phase extraction treatments

Through the water bath to control environmental temperature, Cu-Ni-P ribbons were immersed in 3.2 mol/L ferric chloride aqueous solution. After a period of corrosion operation, Cu in the ribbons would be etched away due to lower reducibility. Subsequently, the residual powders were collected, washed with ethanol and distilled water 5~7 times and put in a vacuum drying set. Finally, the Ni-P samples were collected and systematically characterized.

1.3 Microstructure and phase characterization

The typical microstructural characterizations of ingot-like Cu-Ni-P alloys were carried out using high scope video microscope (HSVM). The phase compositions of precursor alloys were characterized by X-ray diffraction (XRD, D8 Advance) and the corresponding microstructure analysis was conducted by a field emission scanning electron microscope (FESEM, FEI Quanta FEG 250) equipped with energy dispersive X-ray spectrometer (EDS). In addition, the special characterizations of pore structure of Ni-P particles were evaluated from at least five FESEM images of powder samples and in each area about 10 Ni-P products were detected.

2 Results and Discussion

2.1 Phase compositions of Cu-Ni-P alloys

Fig. 1 shows the XRD patterns of types of Cu-Ni-P ingots and melt-spun ribbons. Based on the diffraction peaks in Fig. 1a, it is observed that these Cu-Ni-P ingots are composed of Cu and multiple nickel phosphides with different stoichiometric ratios, including Ni_5P_4, $Ni_{12}P_5$ and Ni_3P. Since chemical activity of element nickel is higher than that of copper, phosphorus in these metallic melts will prefer to react with nickel to form corresponding Ni-P compounds through in-situ reaction. While no other copper phosphides are detected in whole metallic systems. In addition, it is found that the nickel phosphide in Cu-17.1Ni-4.5P ingot (atomic ration of Ni and P as 2∶1) mainly exists in the form of Ni_5P_4 accompanied with trace $Ni_{12}P_5$ according to the intensity of X-ray diffraction peaks. With further increasing the addition levels of element nickel, the phosphides are mainly present in the form of $Ni_{12}P_5$ and Ni_3P compounds which possess relatively higher atomic ratio of Ni and P.

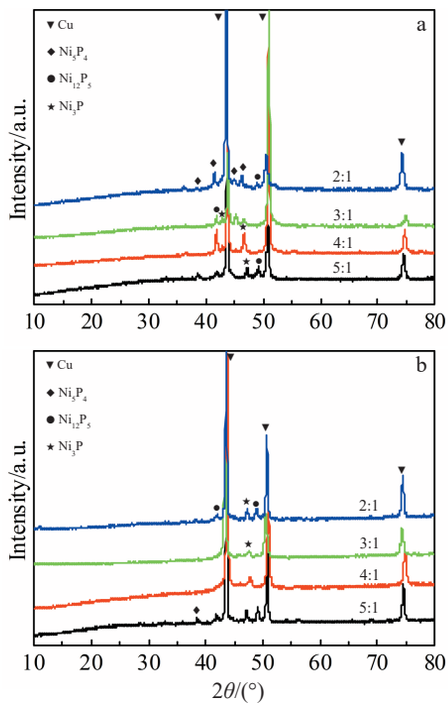

Fig.1 XRD patterns of Cu-Ni-P samples with different Ni∶P ratios: (a) alloy ingots and (b) melt-spun ribbons

As we all know, the melt-spinning technology with extremely high solidification rate sometimes up to 10^4~10^8 K·s^{-1} has obtained a wide application in nanocrystalline and amorphous alloys[24,25], metastable phase synthesis[26], dealloying system precursors[27,28], etc. After melt-spinning process, the corresponding XRD patterns of Cu-Ni-P ribbons are illustrated in Fig. 1b. It is found that the phosphides in ribbons are almost transformed to $Ni_{12}P_5$ and Ni_3P compounds, indicating that the non-equilibrium condition provided by melt-spun treatment may have an obvious influence on the precipitation and growth behavior of phosphides during the solidification process.

2.2 Microstructure characterization of Cu-Ni-P ingots

The typical microstructures of Cu-Ni-P ingots are illustrated

in Fig. 2. As clearly indicated in Fig. 2, besides primary α-Cu matrix, there are lots of grey dendritic compounds, which can be deduced to be nickel phosphides based on XRD analysis in Fig. 1. Due to the rapid solidification rate in vacuum arc melting process, some dendrites grow in a certain direction, as shown in Fig. 2b. Furthermore, with increasing the nickel content from 17.1% to 25.6%, 34.1%, and 42.6%, the average widths of Ni-P dendrites as indicated by dotted lines are about 7.58, 11.11, 15.66 and 20.20 μm, respectively. Based on this, it can be deduced that the higher concentration of nickel will promote the formation and precipitation behavior of Ni-P compounds.

As shown in Fig. 3, FESEM analysis of Cu-34.1Ni-4.5P ingot indicates further identify of dendritic precipitations. It can be seen clearly that the fine lamellar eutectic structure composed of Cu and Ni-P compounds is embedded in Cu matrix, and the partially enlarged detail of eutectic structure is illustrated in the inset of Fig. 3a. From the distributions of element Cu, P and Ni in Fig. 3b~3d, it is found that the solid solution state of Cu and Ni in each other can be clearly detected due to their ultimate mutual solubility. Furthermore, it can also be observed that the distributions of elements Ni and P are rather uniform and the multiple nickel phosphides containing Ni_5P_4, $Ni_{12}P_5$ and Ni_3P cannot be clearly distinguished between each other. Based on the element distritutions for separate element along the line from M to N in Fig. 4a, it is observed that the relative ratio of Ni and P in Ni-P positions fluctuates within a range. Furthermore, the solid solution state of both elements is further proved according to the broad base line of element distribution of Cu and Ni in Fig. 4b and 4d.

The detailed FESEM analyses of Cu-17.1Ni-4.5P ingot are illustrated in Fig. 5. As for Cu-17.1Ni-4.5P ingot, the phosphide mainly takes the form of Ni_5P_4 with a trace amount of $Ni_{12}P_5$ according to XRD analysis in Fig. 1. The atomic ratios of Ni and P in Fig. 5c and 5d are 1.38 and 1.41, respectively, which are in the range of 1.25 (Ni_5P_4) and 2.40 ($Ni_{12}P_5$). Based on this, it can be deduced that the chemical compositions of multiple nickel phosphide dendrites are gradually changed.

2.3 Morphology characterization of Ni-P compounds extracted from ingots

In order to investigate the 3-dimensional (3D) morphologies of Ni-P compounds, the phase extractions of Cu-Ni-P ingots were carried out and the detailed FESEM images of Ni-P particles are shown in Fig. 6. As illustrated in Fig. 6a and

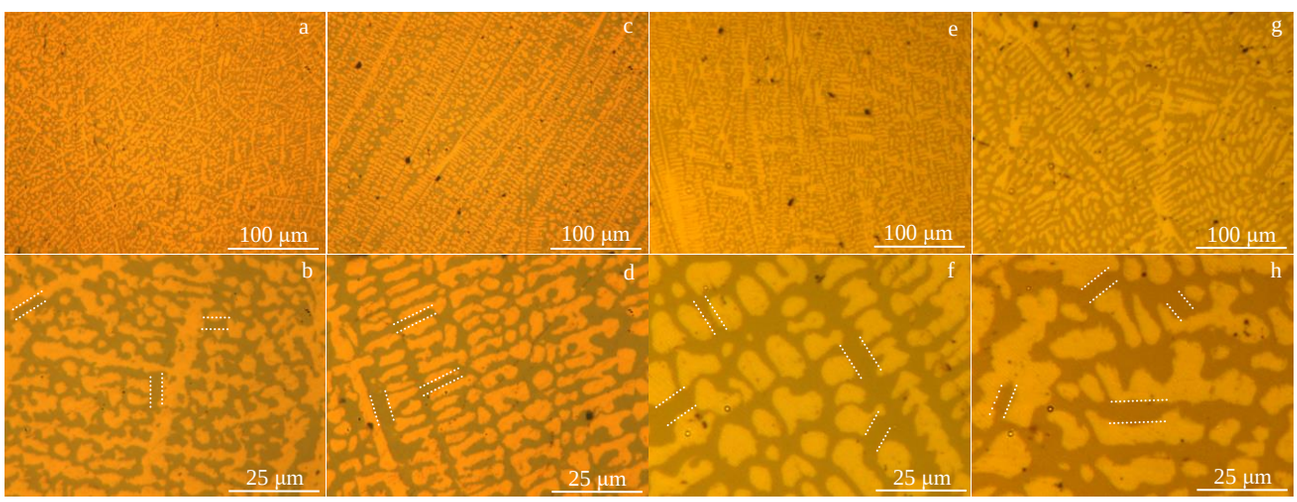

Fig.2 Typical microstructures of Cu-17.1Ni-4.5P (a, b), Cu-25.6Ni-4.5P (c, d), Cu-34.1Ni-4.5P (e, f), and Cu-42.6Ni-4.5P (g, h) ingots with Ni/P atomic ratios of 2:1, 3:1, 4:1 and 5:1

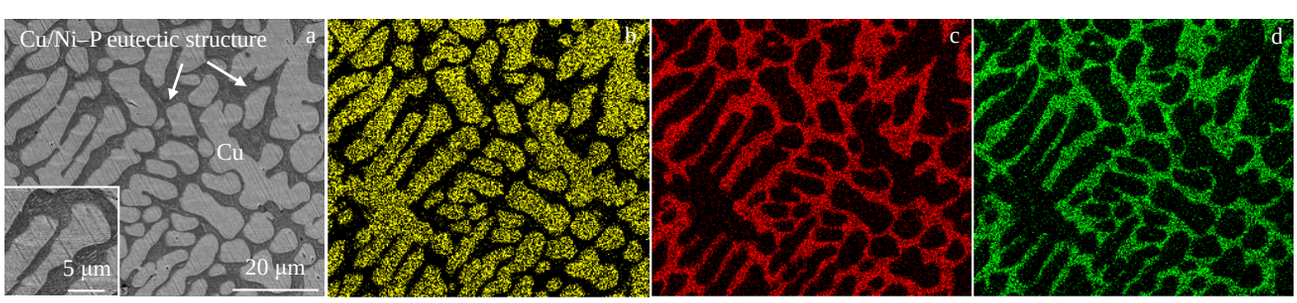

Fig.3 Typical FESEM image of Cu-34.1Ni-4.5P ingots (a) and element distributions of Cu (b), P (c), and Ni (d)

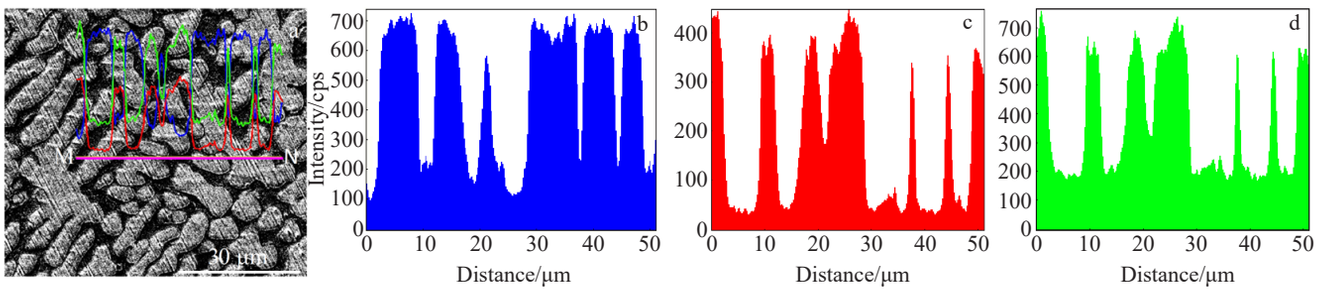

Fig.4 FESEM image of Cu-34.1Ni-4.5P ingot (a) and element distributions of Cu (b), P (c), and Ni (d) along the line from M to N marked in Fig.4a

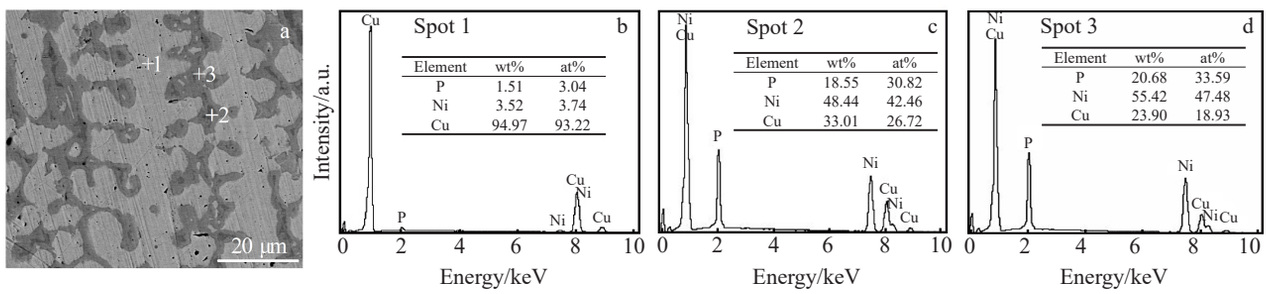

Fig.5 Typical FESEM image (a) of Cu-17.1Ni-4.5P ingot and the results of EDS analyses of spots 1 (b), 2 (c), and 3 (d) marked in Fig.5a

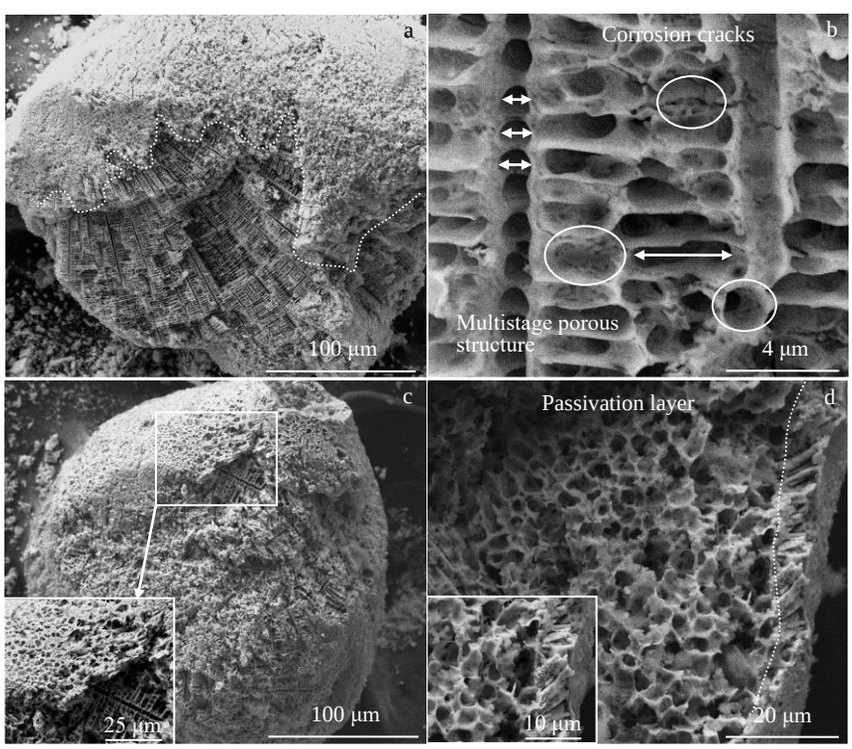

Fig.6 FESEM morphologies of multistage porous Ni-P particles extracted from different Cu-Ni-P ingots at room temperature: (a, b) Cu-25.6Ni-4.5P sample and (c, d) Cu-34.1Ni-4.5P sample

6c, the porous Ni-P particles obtained from Cu-25.6Ni-4.5P and Cu-34.1Ni-4.5P ingots are about 299.58 and 245.42 μm in size, respectively. Furthermore, it is found that the porous structure on the surface layer is slightly different from that within the particles and the exposed interface formed during the phase extraction process is illustrated by the dotted line in Fig. 6a. By statistic analysis for the partial enlargement in Fig. 6b, the macropore diameter mainly decreases within the

range from 0.99 μm to 3.41 μm, as indicated by the arrows. Besides these macroporous regions, plenty of mesopores, as marked by the circles, are also observed with uniform distribution on the ligaments, which are produced by the etching away of Cu within the eutectic structure (Cu+Ni-P). Meanwhile, the removing of Cu in the ligaments may have an influence on the framework stability of Ni-P particles and the corrosion cracks are also observed which might be caused by the corrosion stress. With the increase of solid solution of Cu in Ni-P regions, more Cu atoms need to be removed from the ribbons during the phase extraction process, resulting in more corrosion stresses left. Based on these aspects, the average sizes of Ni-P particles will be reduced due to the development and penetration behavior of cracks. With further increasing the nickel concentration, the anti-corrosion property of Cu-Ni-P alloys will be improved because the self-corrosion potential of nickel is higher than that of Cu. As clearly indicated in Fig.6d, a passivation layer with 3.89~7.16 μm in thickness is detected. Kosinova et al[29] synthesized porous gold nanoparticles covered with a thin and conformal alumina layer and reported that the passive alumina film has an improvement effect on the thermal stability of nanoporous structure. According to the references, element nickel can form a relatively chemically stable passivation layer in air and under many acidic and alkaline environments[30,31]. As for Cu-Ni-P metallic system, ferric chloride aqueous solution is chosen as the etching agent, indicating that these ingots are immersed into acid solution. After the Cu matrix is etched away, Ni-P particles with macroporous structure will be obtained, and then with extending erosion time, more and more Cu in the eutectic structure will be corroded, which is helpful to the formation of pores on the ligaments. Furthermore, the passive film is also detected at the interface between the frameworks and acidic etching solution during the corrosion process.

2.4 Multistage porous Ni-P particles obtained from Cu-Ni-P ribbons

Fig. 7a~7d show the FESEM morphologies of the fracture surface of Cu-Ni-P ribbons. Based on the statistic analysis, the thicknesses of Cu-25.6Ni-4.5P and Cu-34.1Ni-4.5P ribbons is about 21.76 and 23.11 μm, respectively. Through the rapid solidification, the microstructures of Cu-Ni-P ribbons are obviously refined. Meanwhile, it can be observed that the elements Cu, P and Ni are homogeneously distributed in ribbon samples according to the EDS analysis in Fig.7e~7g.

In order to get more information about the phase extraction process, the influence of etching temperature on the powder product of Cu-Ni-P systems was also studied. Fig. 8 shows the typical 3D morphologies of Ni-P particles obtained from Cu-34.1Ni-4.5P ribbons etched at 50 and 80 ℃. It is worth noting that the extraction product has an obvious dependency with the temperature of etching solution. As illustrated in Fig. 8a~8c, with appropriate etching temperature and time, porous Ni-P particles with clear outlines are obtained. The average size of Ni-P particles extracted from Cu-34.1Ni-4.5P ribbons is about 25.37 μm through statistic analysis. Meanwhile, some pores with 63.16~126.32 nm in size are found in the ligaments due to the dissolution behavior of Cu, and small corrosion cracks are also detected, as marked by circles in Fig. 8b and 8c. Based on the rapid cooling rate for alloy ribbons, more Cu can be dissolved into Ni-P regions during the solidification process, which means that more corrosion stresses may be left due to the removing behavior of more Cu in these areas. As corrosion time prolongs, the multistage porous structure of Ni-P ligaments will be ruptured due to the accumulation of corrosion stresses, resulting in obvious decrease of particle size, as illustrated in Fig. 8a. With further increasing the temperature of corrosion solution to 80 ℃, it is found that the Ni-P ligaments become remarkably thinner with the pores becoming larger, which is caused by the improved mobility of atoms due to higher environment temperature. From circles indicated in Fig. 8d, some cleavage planes in the ligaments are clearly observed which may result in a significant reduction in particle size of extracted phosphides. In addition, it is found that for the phase

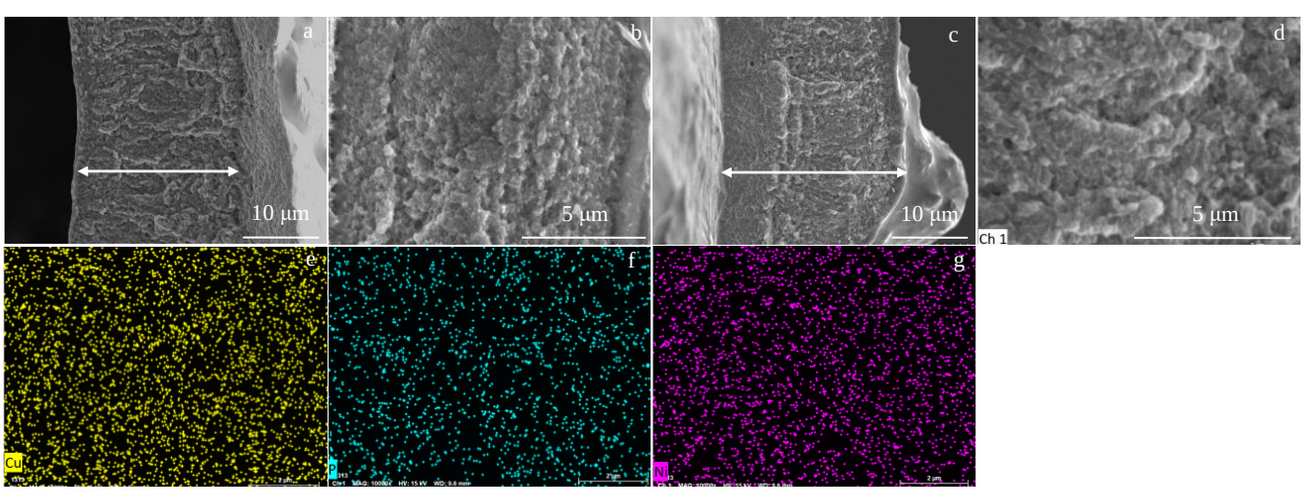

Fig.7 FESEM morphologies of the fracture surface of Cu-25.6Ni-4.5P (a, b) and Cu-34.1Ni-4.5P (c, d) ribbons; corresponding element distributions of Cu (e), P (f) and Ni (g) in Fig.7d

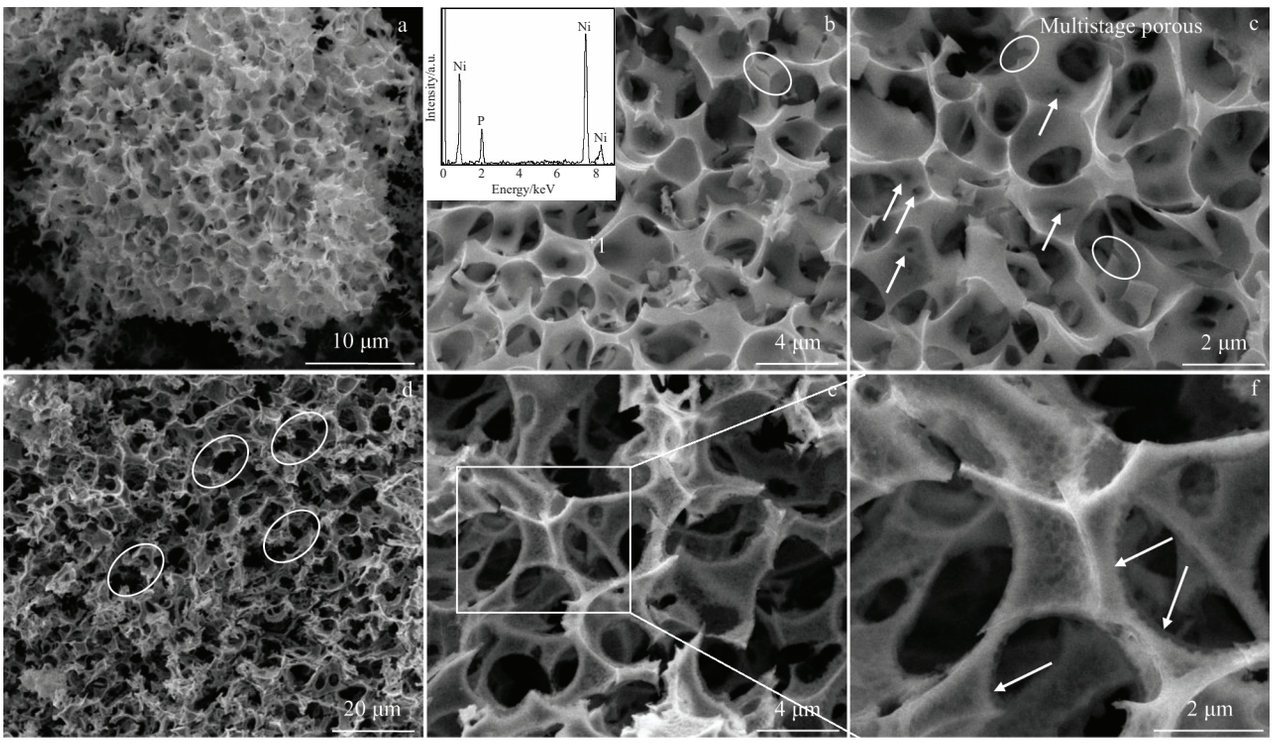

Fig.8 FESEM morphologies of multistage porous Ni-P particles obtained from Cu-34.1Ni-4.5P ribbons etched at 50 ℃ for 4 h (a~c) and 80℃ for 2.5 h (d~f)

extraction at higher temperature, for example 80 ℃ , the formation of passive films adhered to Ni-P frameworks are also observed after etching for only 2.5 h, as illustrated by the arrows in Fig. 8f. Based on this, it can be concluded that the pore structure of Ni-P particles can be tuned through controlling the etching environment, which has a corresponding relationship with the surface diffusivity of substrate[32, 33].

2.5 Formation process of multistage porous Ni-P frameworks

During the melt-spun process, the solidification rate of metallic melt can be significantly increased with the change of rotating speed of Cu roller. In these Cu-Ni-P alloys, the nanoporous Ni_xFe_{1-x}-P hybrid phosphides can be obtained after the extraction treatment of metallic ribbons solidified with 2500 r/min of Cu roller. The typical morphologies of nanoporous Ni_xFe_{1-x}-P particles obtained from Cu-Ni-P ribbons are shown in Fig. 9. As for Cu-17.1Ni-4.5P sample, the nanoporous Ni-P powders are successfully obtained through etching at 50 ℃ for 5 h. With increasing the concentration of Ni in basic alloy, the interconnectivity state of Cu in the metallic alloy is decreased, resulting in the time prolongating for the whole corrosion of Cu dendrites and Cu existing in eutectic structure and solid solution region, as indicating in Fig. 9c. As the corrosion process proceeds, the replacement reaction between Fe and Ni atoms on the ligaments is found due to the higher chemical activity of Fe compared to Ni, which can be proved by the corresponding high content of Fe and P from EDS analysis listed in Fig. 9d. Additionally, it is reported that the bimetallic phosphides might show an activity superior to mono-metallic phosphides due to the synergistic effect[34,35]. Li et al[36] found that the incorporation of Fe into Ni_2P nanosheet arrays as bifunctional catalysts has an improvement effect on the catalytic performance for overall water splitting, which is attributed to the high intrinsic activity and super-aerophobic surface property. Kan et al[37] reported that NiCoP-0.01Fe nanospheres possess excellent bifunctional water splitting catalytic performance and the doping of Fe has an influence on the surface topographies and chemical binding energy, resulting in the evolution of electrochemical performance.

The formation process of multistage porous Ni-P particles obtained from Cu-Ni-P alloys can be deduced as follows. Through the in-situ reaction, Ni reacts with Cu_3P from raw materials to form the corresponding Ni-P compounds, which exhibit typical three dimensional continuous structures. During the extraction process in ferric chloride aqueous solution, Cu matrix of ribbons may be gradually corroded away because of the stronger reducibility of Cu, resulting in the Ni-P compounds left. Furthermore, it is found that the configuration state of Ni-P products can be tuned through the control of basic microstructure of ribbons and corrosive environment. After melt-spinning process, Cu-Ni-P ribbons with rather fine microstructure are immersed in ferric chloride aqueous solution at 50 ℃ for a certain time and phosphides in the ribbons may react with $FeCl_3$ to form the corresponding Fe-P compounds. The high chemistry activity of original

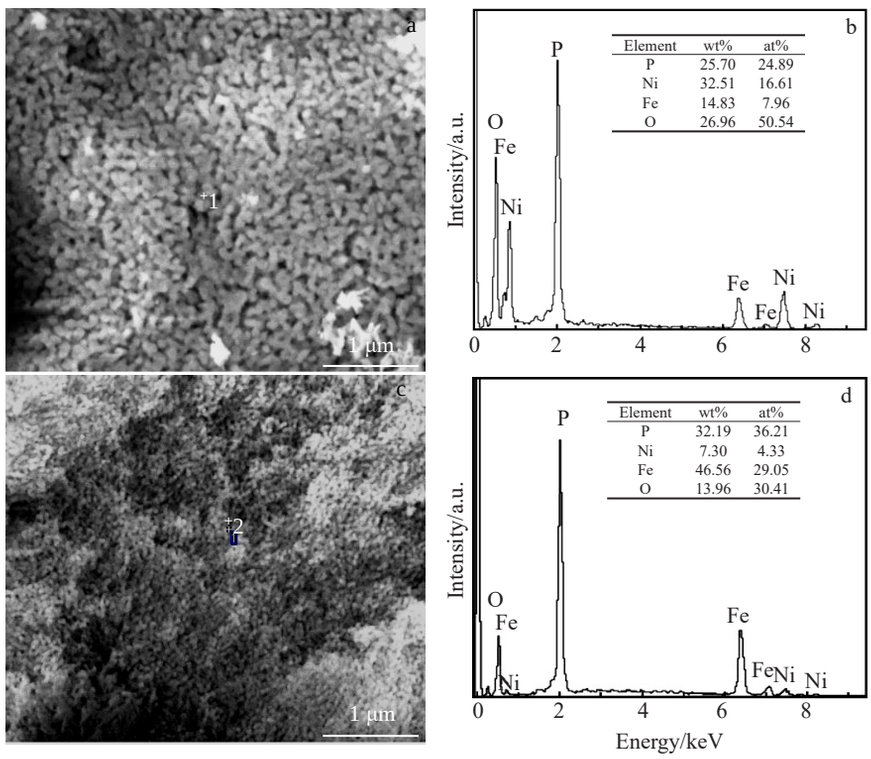

Fig.9 Typical morphologies of nanoporous Ni_xFe_{1-x}-P networks obtained from Cu-Ni-P ribbons: (a) Cu-17.1Ni-4.5P, etched at 50 ℃ for 5 h; (b) results of EDS analysis for spot 1 in Fig.9a; (c) Cu-25.6Ni-4.5P, etched at 50 ℃ for 8 h; (d) result of EDS analysis for spot 2 in Fig.9c

ultrafine structure of Ni-P powders may have an improvement on the replacement behavior between Fe and Ni during this extraction process. The reaction equations of these ribbons during extraction process are listed as follows. Due to the solubility of Fe_2P in hot water, it can be found that FeP compounds will be left in the solution after the long time holding. According to the EDS analysis of product in Fig. 9d, it is found that the relative atomic ratio of Fe and P is about 1.24:1, which is close to the ratio of FeP compound. This further proves the formation of FeP compounds from the phase extraction of Cu-Ni-P ribbons with rather fine microstructure. Furthermore, this appearance also provides a novel route to synthesize Ni_xFe_{1-x}-P phosphides, significantly broadening the application potential of functional phosphides.

$$Cu + 2FeCl_3 = CuCl_2 + 2FeCl_2 \quad (1)$$

$$Ni_3P + 2FeCl_3 = 3NiCl_2 + Fe_2P \quad (2)$$

$$Ni_{12}P_5 + 8FeCl_3 = 12NiCl_2 + 3Fe_2P + 2FeP \quad (3)$$

3 Conclusions

1) Bulk Cu-Ni-P ingots with different atomic ratios of Ni:P (2:1, 3:1, 4:1 and 5:1) are composed of Cu and various Ni-P compounds, including Ni_5P_4, $Ni_{12}P_5$ and Ni_3P. In the melt-spun ribbons, the main existence forms of phosphides change to $Ni_{12}P_5$ and Ni_3P compounds due to the non-equilibrium condition during melt-spun process.

2) Cu-Ni-P systems have similar microstructures, all of which contain Cu matrix and Ni-P dendrites with various stoichiometric ratios. With further increasing nickel concentrations from 17.1% to 42.6%, the microstructures of these alloys have no obvious change.

3) Through the phase extraction process, the multistage porous Ni-P particles can be obtained from Cu-Ni-P ingots, which are formed through the dissolution behavior of Cu dendrites and Cu existing in eutectic structure and solid solution.

4) With rather fine structure of original ribbons, the replacement reaction between Fe and Ni atoms on the Ni-P ligaments can be detected due to the higher chemical activity of Fe than that of Ni, which may provide a novel route to synthesize Ni_xFe_{1-x}-P phosphides and significantly broaden the application potential of functional phosphides.

References

1 Merki D, Hu X L. *Energy and Environmental Science*[J], 2011, 4(10): 3878

2 Kibsgaard J, Tsai C, Chan K, Benck J D. *Energy and Environmental Science*[J], 2015, 8(10): 3022

3 Liang F. *Rare Metal Materials and Engineering*[J], 2018, 47(S1): 269 (in Chinese)

4 Read C G, Callejas J F, Holder C F *et al*. *ACS Applied Materials and Interfaces*[J], 2016, 8(20): 12 798

5 Sun J, Song X X. *Rare Metal Materials and Engineering*[J], 2017, 46(2): 433 (in Chinese)

6 Feng L G, Vrubel H, Bensimon M *et al. Physical Chemistry Chemical Physics*[J], 2014, 16(13): 5917

7 Xu H H, Lu S X, Ren L L. *International Journal of Hydrogen Energy*[J], 2017, 42(29): 18 383

8 Wexler R B, Martirez J M P, Rappe A M. *ACS Catalysis*[J], 2017, 7(11): 7718

9 Mi K, Ni Y H, Hong J M. *Journal of Physics and Chemistry of Solids*[J], 2011, 72(12): 1452

10 Tian S, Li X, Wang A J *et al*. *Angewandte Chemie International Edition*[J], 2016, 128(12): 4098

11 Ledendecker M, Calderón S K, Papp C *et al*. *Angewandte Chemie International Edition*[J], 2015, 127(42): 12 538

12 Liu S D, Sankar K V, Kundu A *et al*. *ACS Applied Materials and Interfaces*[J], 2017, 9(26): 21 829

13 Xiang J Y, Wang X L, Xia X H *et al*. *Journal of Alloys and Compounds*[J], 2011, 509(1): 157

14 Ding Y, Kim Y J, Erlebacher J. *Advanced Materials*[J], 2004, 16(21): 1897

15 Han J H, Li C, Lu Z *et al*. *Acta Materialia*[J], 2019, 163: 161

16 Wittstock A, Zielasek V, Biener J *et al*. *Science*[J], 2010, 327(5963): 319

17 Chen J, Lian L X, Liu Y *et al*. *Rare Metal Materials and Engineering*[J], 2019, 48(10): 3088

18 Mu Z Y, Zhou X L, Fan Z *et al. Rare Metal Materials and Engineering*[J], 2019, 48(10): 3252 (in Chinese)

19 Chen L Y, Yu J S, Fujita T *et al*. *Advanced Functional Materials* [J], 2009, 19(8): 1221

20 Qiu H J, Kang J, Liu P *et al*. *Journal of Power Sources*[J], 2014, 247: 896

21 Hakamada M, Mabuchi M. *Journal of Alloys and Compounds*[J], 2009, 479(1-2): 326

22 Tan Y W, Wang H, Liu P *et al*. *Advanced Materials*[J], 2016, 28(15): 2951

23 Tan Y W, Wang H, Liu P *et al*. *Energy and Environmental Science*[J], 2016, 9(7): 2257

24 Zhai S C, Peng Z R, Guan Y F *et al. Journal of Non-Crystalline Solids*[J], 2019, 506: 28

25 Si J J, Du C X, Wang T *et al*. *Journal of Alloys and Compounds* [J], 2018, 741: 542

26 Kenel C, Leinenbach C. *Journal of Alloys and Compounds*[J], 2015, 637: 242

27 Xu C X, Hou J G, Pang X H *et al*. *International Journal of Hydrogen Energy*[J], 2012, 37(14): 10 489

28 Mihailov L, Redzheb M, Spassov T. *Corrosion Science*[J], 2013, 74: 308

29 Kosinova A, Wang D, Baradács E *et al*. *Acta Materialia*[J], 2017, 127: 108

30 Lambers E S, Dykstal C N, Seo J M *et al*. *Oxidation of Metals* [J], 1996, 45: 301

31 Lührs L, Weissmüller J. *Scripta Materialia*[J], 2018, 155: 119

32 Dan Z H, Qin F X, Sugawara Y *et al*. *Microporous and Mesoporous Materials*[J], 2014, 186: 181

33 Dan Z H, Qin F X, Yamaura S *et al*. *Journal of Alloys and Compounds*[J], 2013, 581: 567

34 Luo J S, Steier L, Son M K *et al. Nano Letters*[J], 2016, 16(3): 1848

35 Ilyas T, Raziq F, Ali S *et al*. *Applied Surface Science*[J], 2021, 543: 148 726

36 Li Y J, Zhang H C, Jiang M *et al*. *Advanced Functional Materials*[J], 2017, 27(37): 1 702 513

37 Kan S T, Xu M Y, Feng W S *et al*. *ChemElectroChem*[J], 2021, 8(3): 539

典型Cu-Ni-P合金体系物相提取合成多孔结构Ni-P颗粒

左　敏，李永丽，夏文丽，赵德刚，王　艳

(济南大学 材料科学与工程学院，山东 济南 250022)

摘　要：基于不同Ni、P原子比设计合成了Cu-Ni-P系列合金，并针对其特有的微观组织及物相提取过程进行了研究。研究发现，Cu-*x*Ni-4.5P合金铸锭内含有Cu和多种Ni-P物相，如Ni_5P_4、$Ni_{12}P_5$及Ni_3P。经过熔体旋淬处理后，其薄带试样中磷化物主要以$Ni_{12}P_5$和Ni_3P形式存在。此外，对比发现，合金内镍含量的增加在一定程度上促使了磷化物相的粗化。通过调控合金的凝固行为及物相提取工艺，可获得多级孔结构的Ni-P颗粒，其孔洞是由于腐蚀过程中铜基体、共晶组织内及固溶部分的铜被去除而形成的。通过对典型合金进行物相提取，实现了可控合成磷化物，这对于拓展功能性磷化物的应用具有促进作用。

关键词：过渡金属磷化物；Ni-P；微观结构；多级孔；物相提取

作者简介：左　敏，女，1981年生，博士，副教授，济南大学材料科学与工程学院，山东 济南 250022，E-mail：mse_zuom@ujn.edu.cn